Optimizing and Fabricating QDSSCs

By Marwah Sabrah

TABLE OF CONTENTS

TABLE OF FIGURES

1 INTRODUCTION

1.1 QUANTUM DOT-SENSITIZED SOLAR CELL DESIGN

The emergence and development of quantum dot-sensitized solar cells (QDSCs) over the past two decades has shown its promise as an inexpensive, large-scale, high durability alternative to efficient renewable energy. The QDSC design borrows heavily from dye-sensitized solar cells (DSCs) which use a molecular dye rather than quantum dots (QDs) as the light absorber (sensitizer). QDs are incredibly advantageous as sensitizers, as they exhibit phenomenal fluorescence properties, an easily tunable bandgap by size control which allows harvesting UV light (atypical for traditional semiconductors), high extinction coefficients, and a large intrinsic dipole moment which allows rapid charge separation. These characteristics make QDs good sensitizers because have high photon absorption and easily adjustable properties for the wavelengths of light absorbed.

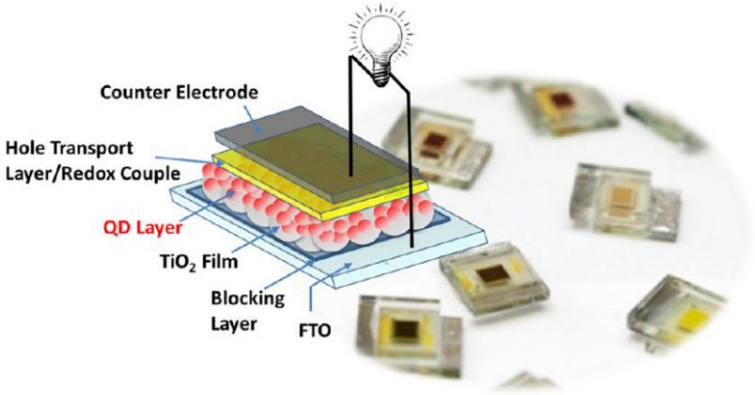

Figure 1.1: Diagram of layers in a QDSC

Source: [1]

To fabricate a functional QDSC, the fundamental components include two electrodes, a sensitizer-loaded mesoporous metal oxide (commonly TiO_2), and an electrolyte containing a redox system. Additional layers are explored in QDSC literature and are optional to increase cell efficiency as discussed in section 1.2. The configuration of a QDSC is illustrated in above in Figure 1.1.

First, photons via sunlight enter the quantum dot solar cell and strike the **QD Layer.** While the light can enter from any direction which is optically transparent, photons are most efficiently absorbed when light strikes through the photoanode because it is the shortest pathway to the TiO_2 layer and to the quantum dots. The QDs serve as the light absorbers in a QDSC to convert incident photons to into excited electrons. Based on the bandgap of the QDs and the wavelength of the photons, electrons are excited to a higher energy level.

The electrons are then injected into the **Active TiO_2 Layer** which is a 5-10um thick mesoscopic oxide film, usually made of 15-20nm nanoparticles. This electron travel from the QDs to the TiO_2 layer occurs because the electrons are photo-excited and are incentivized to jump from the QD conduction band to the higher TiO_2 conduction band.

The electrons then travel from the TiO_2 layer through the conductive **FTO photoanode** to an external circuit to do useful work**.** This transport across the conductive surface occurs because electrons have a natural tendency to balance charge difference by flowing to the side with less negative charge. Since there is an accumulation of electrons in the TiO_2 layer, the electrons naturally flow through the external circuit where there is less negative charge. The role of the photoanode is that it is a conductive slide, so it allows electrons to transport through it.

Through this process, electrons have left the QD layer and there are now holes remaining there instead—this is where the electrolyte becomes useful. The **Hole Transport Layer/Redox Couple** is made of an electrolyte consisting of two reagents, one serving as an electron donor and the other as an electron acceptor. This electrolyte redox couple acts as a hole transport layer and its role is to fill holes in the QD layer. The electron donor of the redox couple donates electrons to fill the new holes in the QD Layer which results in an electron deficiency in the electrolyte.

While it is possible to use a single species such as S^{2-} which would become S_n^{2-} after its electron donation, research has shown that the addition of a sulfur salt S leads to the formation of polysulfide as well as supersulfide ($S_2^{\cdot-}$) which acts as a far superior redox couple for QDSC performance.

The role of **Counter Electrode** is to replenish electrons for the oxidized electrolyte. The counter electrode achieves this by supplying the electrolyte with the electrons that have flowed through the external circuit and to the counter electrode. The electron acceptor of the redox couple harvests these electrons from the counter electrode. The polysulfide acts as the electron acceptor from the counter electrode through this reaction:

$$S_x^{2-} + 2e \rightarrow S_{x-1}^{2-} + S^{2-}$$

Ultimately, this process creates a voltage difference across the photoanode and the counter electrode. The voltage difference and the direction of current are set by the transportation pathway of the electrons. When electrons in the quantum dots are excited, they must travel somewhere. The reason they travel to the TiO_2 layer is because its conduction band accommodates higher energy and is favorable. While a smaller percentage of electrons do flow backwards to reduce the oxidized electrolyte, there are still enough electrons jumping to the TiO_2 layer to create a current flow in that direction. Additionally, as discussed later in this paper, a blocking layer can be added after the TiO_2 layer to prevent electron backflow. After reaching the TiO_2 layer, electrons travel forward through an external circuit because they have a natural magnetic incentive to flow to the areas with least negative charge. From there, electrons reach the counter electrode and are sent to reduce the oxidized electrolyte. There is no net consumption of material, so the process is regenerative.

1.2 Improving Efficiency

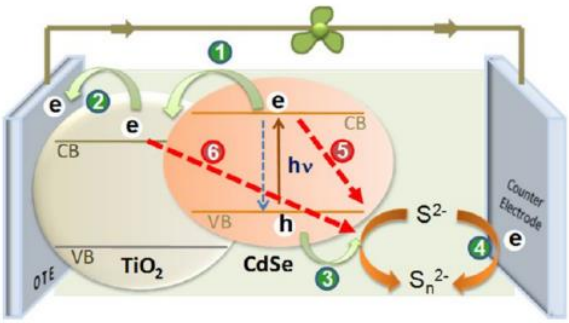

Figure 7. Schematic illustration of photoinduced charge-transfer processes following a laser pulse excitation: (1) Charge injection from excited CdSe into TiO_2; (2) transport of electrons to the collecting electrode surface; (3) hole transfer to the redox couple; (4) regeneration of the redox couple; (5) recombination of electrons from CdSe and the oxidized form of the redox couple; and (6) interfacial recombination of electrons from TiO_2 and the oxidized form of the redox couple. (Reproduced from ref 2.)

Figure 1.2: QDSC charge-transfer process

Source: [1]

While QDSCs and DSCs are similar, their variations in charge, size, and recombination routes mean that the optimized parameters for DSCs do not necessarily translate to QDSCs. Recent QDSC literature has focused on best practices for maximizing its PCE, adopting methods from DSCs and innovating the rest. QDSC efficiency ultimately depends on photoinduced charge separation in QDs, their rapid transport and accumulation in the TiO_2 film, and ultimate delivery to the counter electrode. The limiting factor during this transport is the charge-transfer kinetics of the hole transfer, which is 2-3 orders of magnitude slower than electron transfer between the QD and the TiO_2. Figure 1.2 illustrates this process, showing recombination losses play a major role in limiting efficiency.

1.2.1 Compact TiO_2 Layer

The **Compact TiO_2 Layer** in the TiO_2 film creates a barrier between the FTO and the QD Layer to prevent short circuiting. An additional compact layer of TiO_2 of 10-100nm can be added before the active TiO_2 layer to prevent electron recombination; this back electron transfer results in a short circuit at the photoanode/electrolyte interface leading to a loss of electrons and a decrease in cell stability and PCE. The compact TiO_2 acts as a physical barrier and acts a blocking layer.

1.2.2 Scattering Layer

The **Scattering TiO_2 Layer** employs large particles to scatter light and improve the optical absorption of the incident light. An optional scattering layer is cast after the active TiO_2 layer to provide backscatter photons to the QD sensitizer. This layer increases light absorbance of the solar cell and is created similarly to the active layer, except using larger 400nm anatase TiO_2 particles [2].

1.2.3 Blocking Layer

An additional **Blocking Layer** prevents recombination at the sensitizer/TiO2 and electrolyte interface. Ordinarily, this interaction results in large PCE loss and device instability through the loss of electrons in the FTO conduction band to the electron acceptor in the electrolyte.

In addition to the compact TiO_2 blocking layers discussed above, multiple blocking layers may be introduced after QD deposition to further prevent back electron transfer from the sensitizer (QDs) and TiO_2 particles into the redox couple. The blocking layer minimizes recombination losses at grain boundaries.

2 RESULTS & DISCUSSION

2.1 COLLOIDAL QUANTUM DOTS

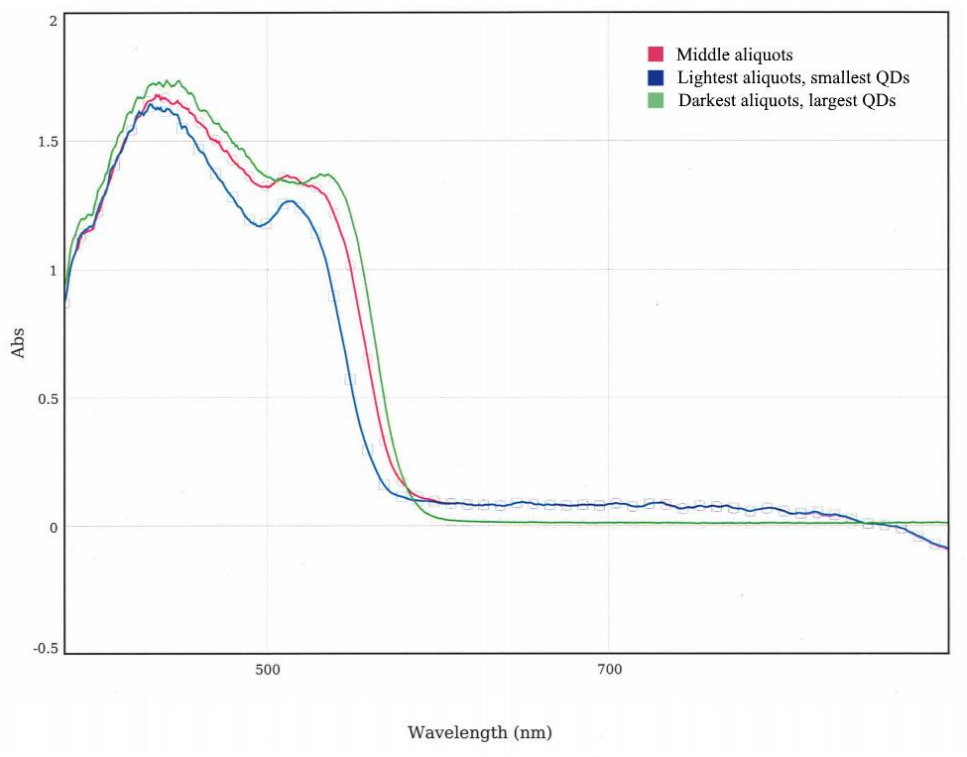

Figure 2.1: Absorption spectra of colloidal CdSe quantum dot solution directly after synthesis

Directly after synthesis, the absorption spectrum of the colloidal CdSe quantum dot solution was recorded as illustrated in Figure 2.1. As described in more detail in Section 6.1, during synthesis the reaction was quenched by isolating small aliquots over the course of approximately 15 seconds. Since there is a small difference in time between the first aliquot quenched and the final aliquot quenched, we expect the size of the final aliquot to be slightly larger than that of the first one. Accordingly, the first aliquot would be a lighter color with a lower peak absorption wavelength whereas the final one would be slightly darker with a higher peak absorption. The data shows the first aliquot has a peak absorption of 514.9nm, the middle aliquot also has a peak absorption of 514.9nm, and the final aliquot has a peak absorption of 534nm. The aliquots were later all combined into one tube.

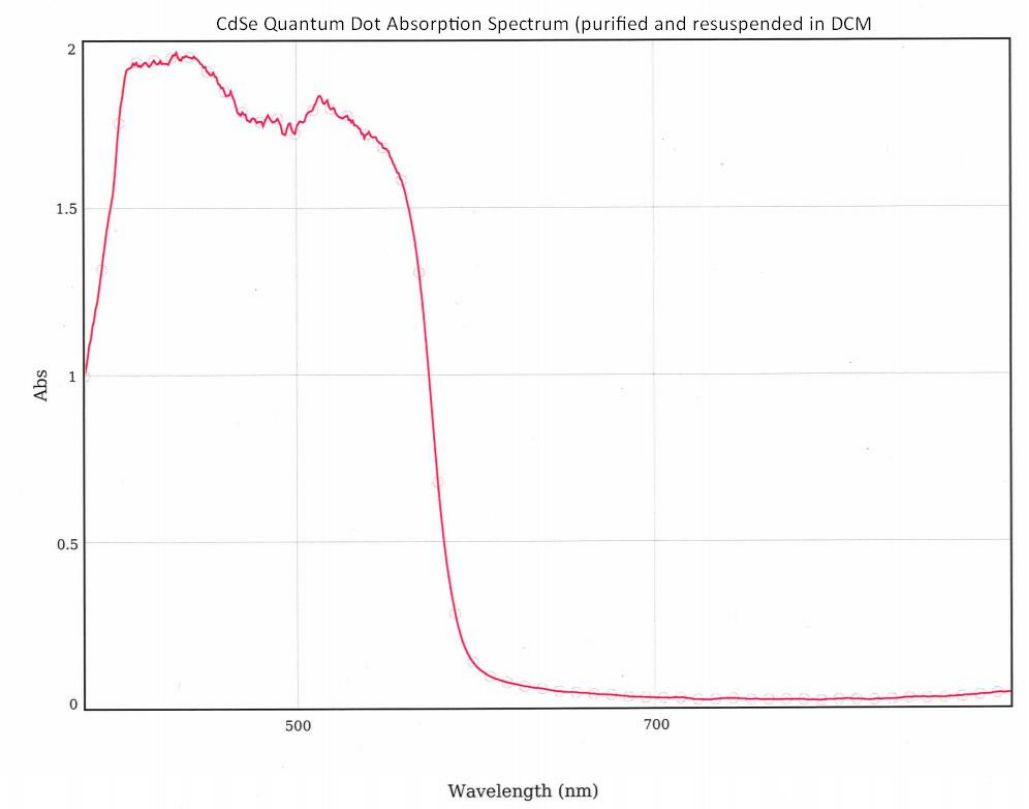

Figure 2.2: Absorption spectra of colloidal CdSe quantum dots after purification and resuspension in dichloromethane

After purification and resuspension of the combined quantum dots in dichloromethane, the absorption spectrum was recorded again. Figure 2.2 illustrates the peak absorption at 513.3nm. Using $E = \frac{h*c}{\lambda}$ we find this corresponds to an energy of 2.4154 eV or 233 kJ/mole.

For a CdSe quantum dot, the particle size D(nm) can be determined by the equation specified in [3]:

$$D = (1.6122 \times 10 - 9)\lambda^4 - (2.6575 \times 10 - 6)\lambda^3 + (1.6242 \times 10 - 3)\lambda^2 - (0.4277)\lambda + (41.57)$$

The spectroscopy data above shows that peak wavelength for the QDs varies from 513 to 535nm, thus the particle sizes vary from 2.5nm to 2.77nm.

The transition energy ΔE is given by absorption peak as mentioned above, thus ΔE varies from 2.41 eV to 2.32 eV. The extinction coefficient for CdSe QDs specified by [3] is given as:

$$\varepsilon = 1600 * \Delta E * D^3$$

Therefore, the extinction coefficient varies from 60250 to 78894 cm^{-1} M^{-1}. Quantifying the extinction coefficient is useful because it characterizes the material properties of the quantum dots synthesized, particularly regarding absorption and penetration of light.

We also attempt to estimate the molar mass of our synthesized quantum dot crystals by relating our calculated particle size to density. If we take the average particle size to be 2.6nm, we can estimate the

volume of each crystal using $V = \frac{4}{3} * \pi * r^3$ where r is 1.3nm. The average particle volume is then 9.2 x 10^{-21} cm^3. Given that CdSe density is 5.81 g cm^{-3}, we find that our quantum dot crystals have a mass of 5.34 x 10^{-20} grams per QD or 32.198 kg/mol.

2.2 TiO_2 Layer

Unfortunately, there were some difficulties with some of the TiO_2 cast layers. While some layers formed seemingly homogenously and intact, most came out of the oven with many cracks that would decrease expected PCE. To characterize the TiO_2 films that we created, we examined their properties under an optical microscope, an optical profiler, and with Scanning Electron Microscopy (SEM).

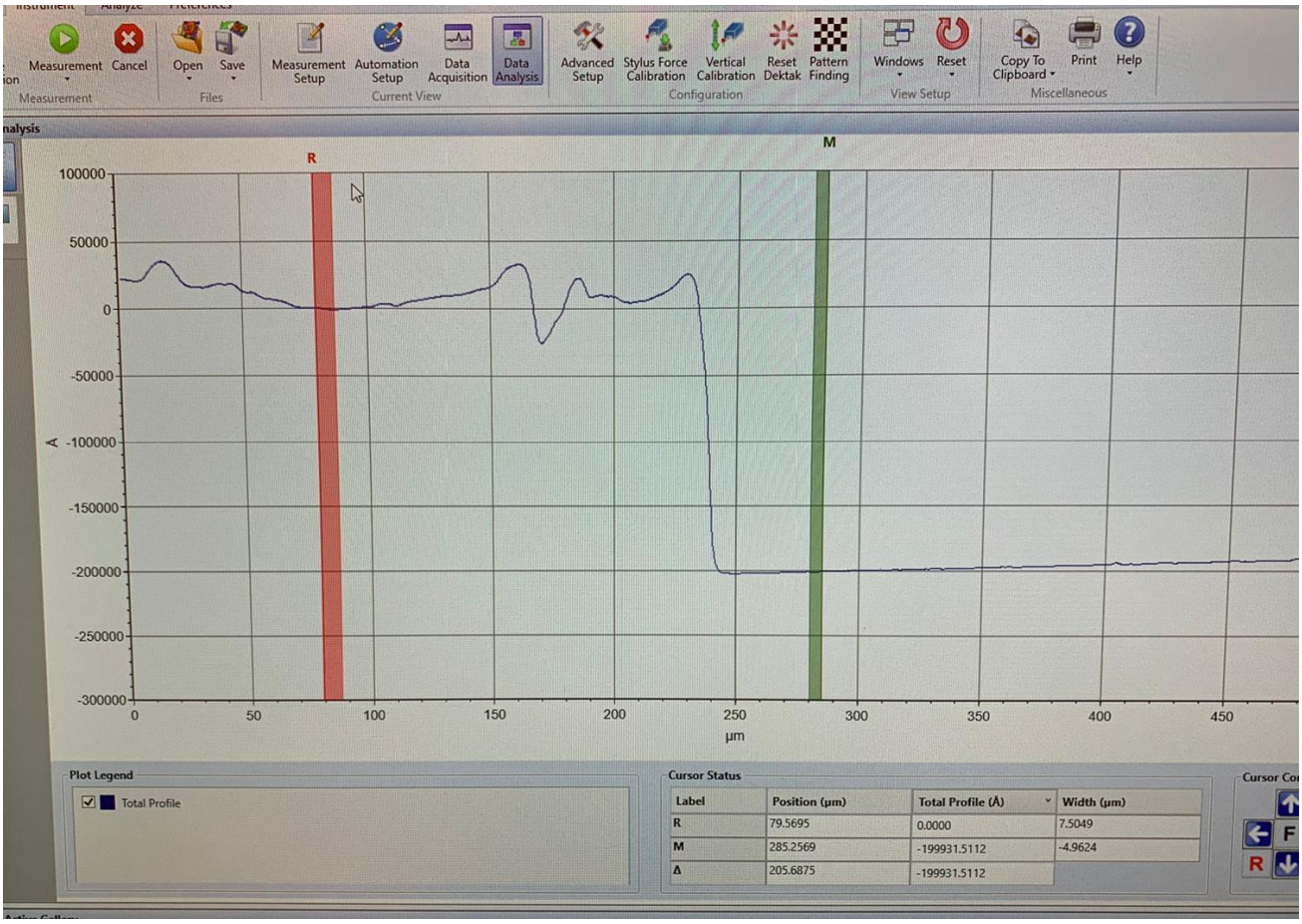

Figure 2.3: Data recorded of TiO2 films under an optical profiler.

Under the optical profiler, we found that the thickness of our TiO_2 layer was approximately 20um as shown in Figure 2.3. This is not drastically far from the recommended thickness in most literature which is approximately 10um.

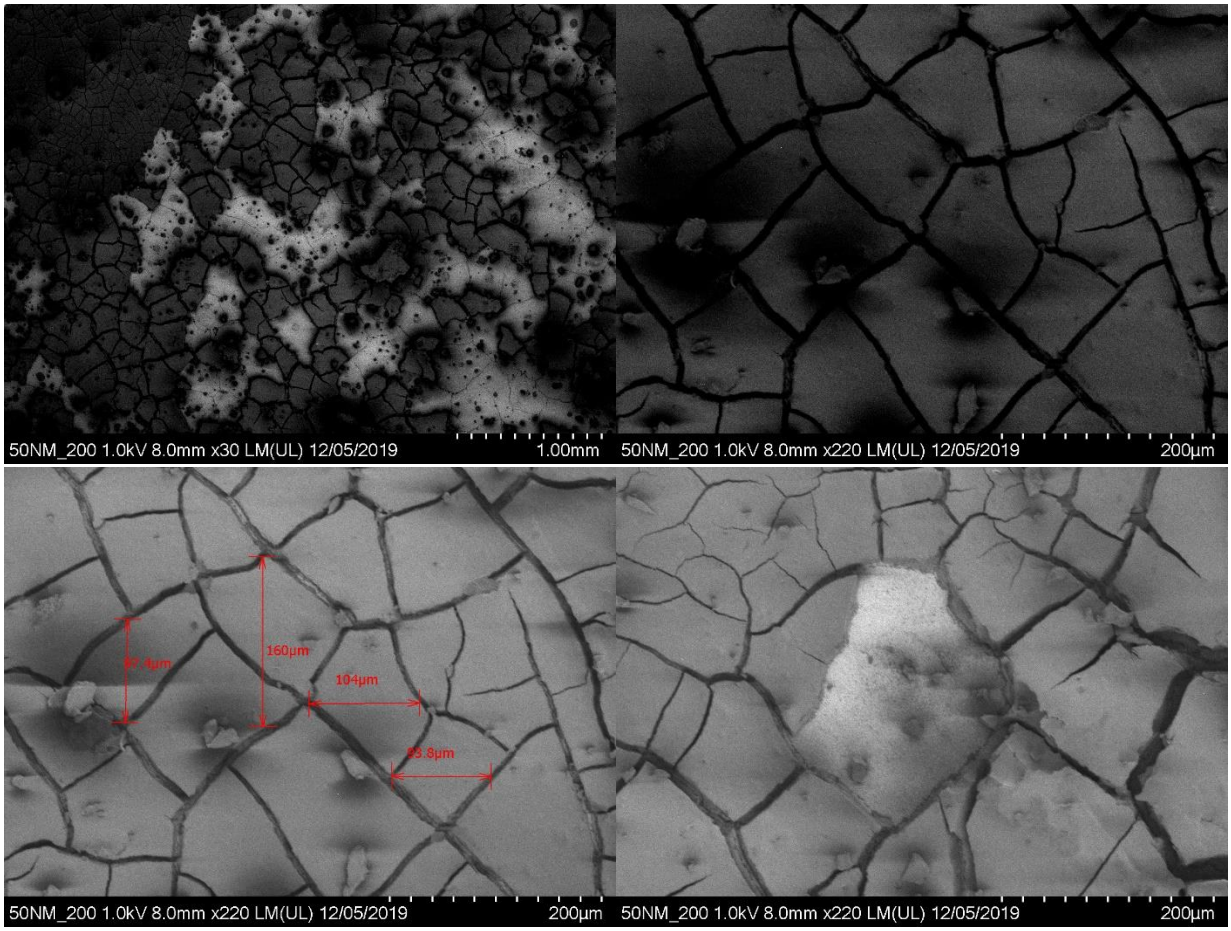

Figure 2.4: Imaging of TiO2 layers using Scanning Electron Microscopy

Furthermore, imaging of the TiO_2 layers with SEM allows us to add to our qualitative understanding of the thin film as shown in Figure 2.4. As shown above, the average distance between cracking in the TiO_2 layer ranged from 90um to 160um. We expect that this cracking reduces the efficiency of electrons traveling through the TiO_2 layer to the photoanode.

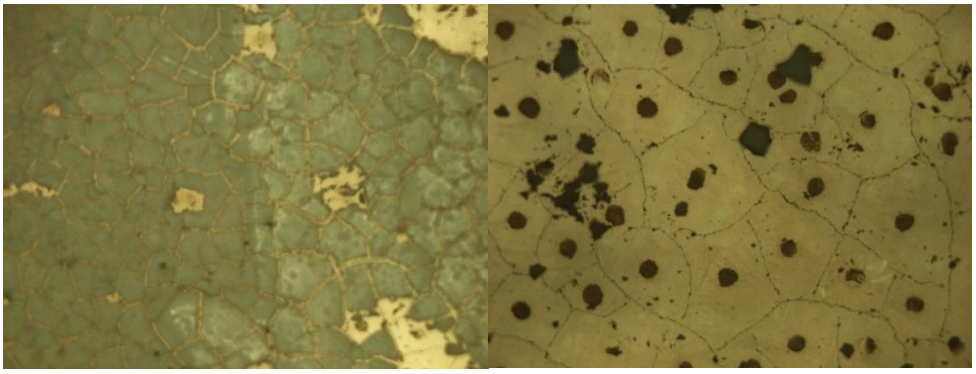

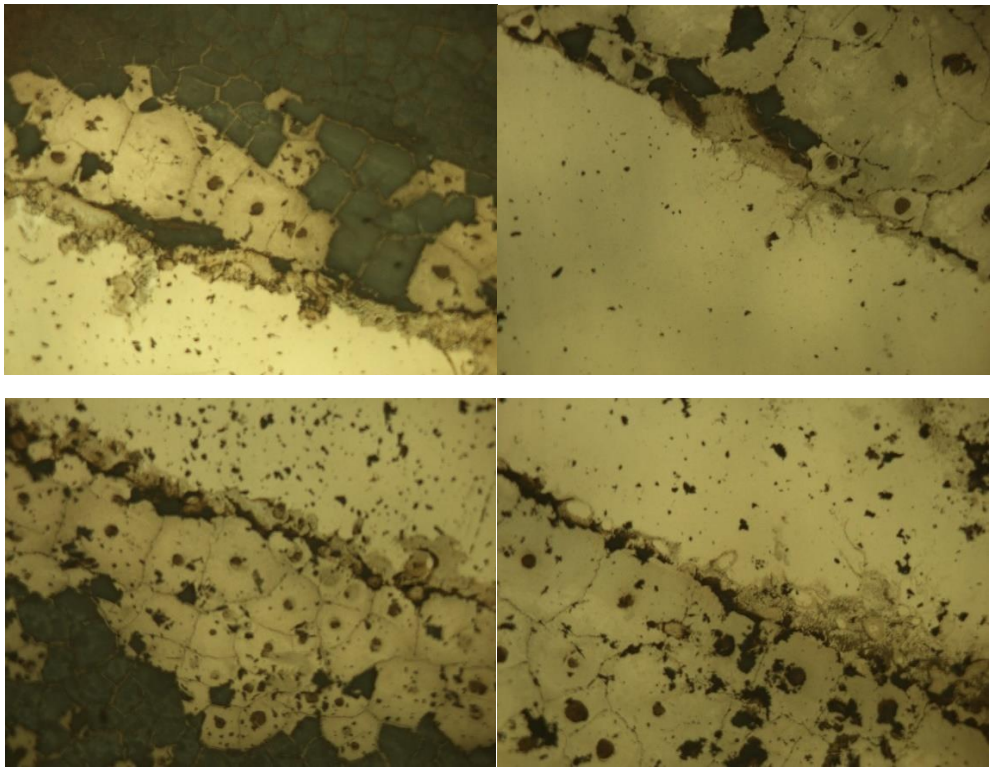

Figure 2.5: Imaging of the TiO2 layer under an optical microscope. On the top left, the center of a TiO2 layer that is intact and solid. On the top right, the center of a TiO2 layer that had washed off. On the middle left, the left edge of a TiO2 layer that is solid. On the middle right, the left edge of a TiO2 layer that had washed off. On the bottom left, the right edge of a TiO2 layer that is solid. On the bottom right, the right edge of a TiO2 layer that had washed off.

The imaging from the optical microscope shown in Figure 2.5 reveals that even after the degradation and washing off of the TiO_2 layer, there are still very sparse remnants of TiO_2 particles attached to the conductive slide. Again, very visible are the cracks in the TiO_2 layer and the rough edges where the layer ends. The high fraction of cracks and gaps in the TiO_2 layer make it a less effective electron transporter and may reduce the concentration of the loaded sensitizer. Therefore, we would expect a less stable device and lower potential output than from a homogenous layer.

2.3 Solar Cells Device Output

As discussed in section 6.8, the solar cell samples were exposed to a light bulb with illuminance of 765 lux or 0.00011169 watts/cm^2. The active area of each solar after assembly was 2.25 cm^2, resulting in input power (P_{in}) of 0.0002513 watts.

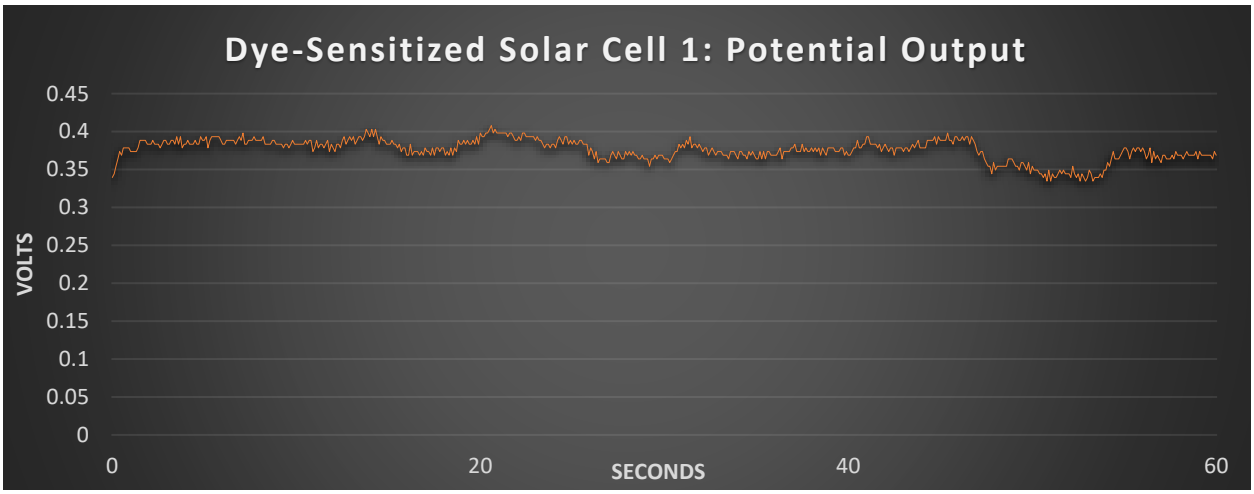

Figure 2.6: Voltage of sample 1 under 250V 600W lightbulb. Average device output is 0.38V.

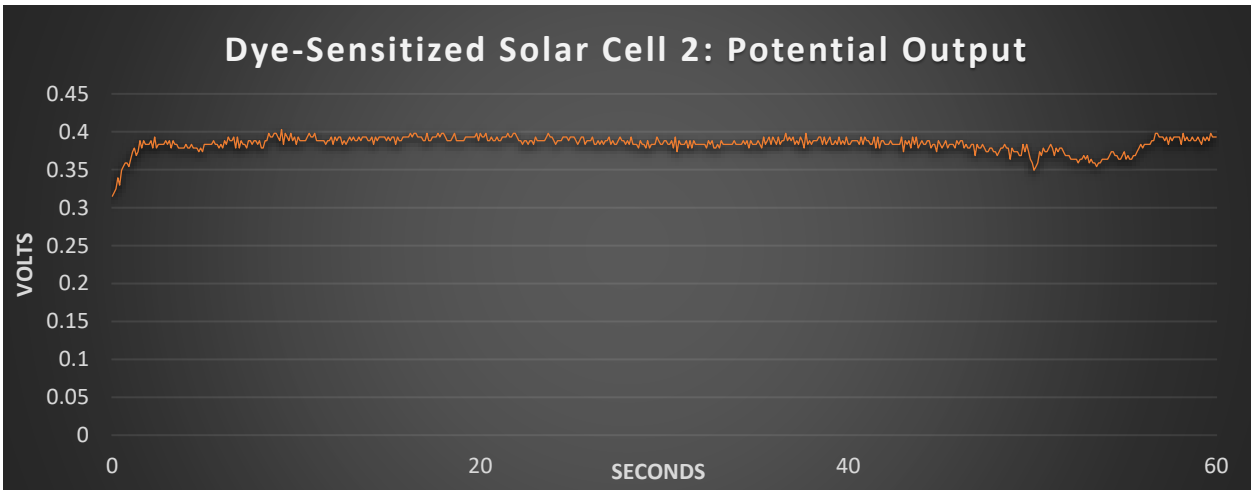

Figure 2.7: Voltage of sample 2 under 250V 600W lightbulb. Average device output is 0.38V.

To start, we assembled 2 dye-sensitized solar cells with an iodide electrolyte and a graphite counter electrode to confirm that the solar cells would function reliably and produce a steady voltage under the specified light. The voltage produced was recorded over 60 seconds as illustrated in Figure 2.6 and Figure 2.7. Both samples produced an average voltage of 0.38V.

Subsequently, we constructed 9 dye-sensitized solar cells and 7 quantum dot-sensitized solar cells each with variations designed to improve efficiency. We measured the voltage produced by every solar cell under both ambient light and the light bulb. For 3 of the samples that showed a non-negligible difference in output voltage from ambient light to the light bulb, we recorded an IV curve to be able to calculate open circuit voltage (V_{OC}), short circuit current (I_{SC}), maximum power (P_{Max}), fill factor (FF), and cell efficiency. However, interestingly, none of the IV curves generated by our samples followed the expected shape of an IV curve for a solar cell which posed a few challenges to making the above calculations. Table 1 below summarizes the solar cells constructed and their properties, including the output voltage of the device.

	Electrolyte Couple	Counter electrode	Blocking Layer	Scattering Layer	Voltage Dark	Voltage Ambient	Voltage Light
**DSC_1*	Iodide	Graphite			Fluctuates	0.94V, decreasing	0.6V, decreasing
DSC_2	Iodide	Graphite			0.026V	-0.025V	3.1V, decreasing
DSC_3	Iodide	Graphite				0.22V	0.76V
DSC_4	Polysulfide	Graphite				0.073V	0.2V
DSC_5	Iodide	Graphite				0.3V	0.55V
DSC_6 (same as DSC_5)	Iodide	Silver				0.01V	Same as ambient
**DSC_7*	Iodide	Graphite				0.01V	0.32V
DSC_8	Iodide	Graphite	ZnS			0.2V	0.65V
DSC_9	Iodide	Copper Sulfide				0.01V	Same as ambient
QDSC_1	Polysulfide	Graphite			0.04 to 0.11	Same as dark	1.5V, decreasing
QDSC_2	Polysulfide	Silver			0.005V	0.004V	0.005V
**QDSC_3*	Iodide	Silver				0.7V	0.36V
QDSC_4	Iodide	Silver		2^{nd} TiO2 layer		0.24→0.6V increasing	Same as ambient
QDSC_5	Iodide	Graphite	ZnS			0.02V	0.19V
QDSC_6	Iodide	Silver	ZnS			0.7V to 1.1V	0.0V
QDSC_7	Iodide	Copper Sulfide				0.01V	Same as ambient

Table 1: Summary of the variations of solar cells constructed and their corresponding voltage outputs.

Samples DSC 1, DSC 2, DSC 3, DSC 5, and DSC 7 are all iterations of the same model: a dye sensitized solar cell with a graphite counter electrode and iodide electrolyte. We took many iterations of this model because we found the output voltage varied drastically and behaved interestingly. Oddly, sample DSC 1 had a higher output voltage under ambient light than under a light bulb—this is very unexpected, given the ambient light is far weaker and would excite fewer electrons. Another odd observation was that the output voltage seemed to steadily decrease with time. Sample DSC 2 also experienced this decreasing phenomenon. Even though sample DSC 2 had a more predictable ambient output voltage (approximately 0), the output voltage under a light bulb was magnitudes higher than what we were expecting. Normally, this model would produce an output voltage between 0.2V and 0.5V, so a 3.1V output was shocking to see, however it did decrease linearly with time. On the other sample, samples DSC 3, DSC 5, and DSC 7 seemed to behave normally.

To be able to objectively compare the effect of using a silver counter electrode on a DSC rather than a graphite counter electrode, we use sample DSC 5. Sample DSC 5 is a dye sensitized solar cell with a graphite counter electrode. The ambient voltage produced is 0.3V and under a light bulb increases to 0.55V. Immediately after collecting this data, the graphite electrode on the sample was swapped with a

silver counter electrode and was labeled as DSC 6. Once the silver counter electrode is swapped, the solar cell stops functioning and produces approximately 0V under both ambient light and a light bulb.

We found that the copper sulfide electrode in both sample DSC 9 and sample QDSC 7 did not produce any significant voltage under a light bulb. We are unsure if this trend would have continued with the use of a polysulfide electrolyte instead, or whether we had successfully created a Cu_2S layer on our original brass sheet.

A few of the QDSC samples also behaved in odd and interesting ways. Sample QDSC 1 demonstrates a high voltage output of 1.5V but then steadily decreases with time. When the counter electrode is switched to silver, the solar cell stops functioning similarly to sample DSC 6. However, in sample QDSC 3, we switch the electrolyte and find that the cell begins functioning again. We find that using a QD-sensitizer with iodide electrolyte (instead of polysulfide) is actually compatible with the silver counter electrode. Weirdly, the ambient output voltage is twice as high as the voltage under a light bulb, but nonetheless the voltages produced are significant. By adding a scattering layer to this model as done in sample QDSC 4, we find that the solar cell no longer behaves as light-sensitive. Instead, a 0.24V is initially produced and grows linearly with time. After 20 minutes, the output voltage increased to 0.6V and was still growing. This was fascinating but very unexpected.

In sample QDSC 5, we use iodide electrolyte with a graphite counter electrode, and this time we add a ZnS blocking layer. We find that the output voltage does increase with light exposure, however very minimally. Shockingly, by switching the counter electrode from graphite to silver, the cell begins to act like a “reverse” solar cell. Under a light bulb it produces 0V, but under ambient light and darkness it produces an output voltage ranging from 0.7V to 1.1V.

We are unsure of what the explanation may be for why many of these samples have decreasing or fluctuating output voltages. One theory we had is that the potential difference may be due to a electrochemical reaction occurring, however this does not necessarily explain some of the other samples which had an output voltage that switched signs between negative and positive. We are baffled by the fascinating results of sample QDSC 4 which did not seem light sensitive but experienced a constant increase in output voltage with time; if there were fewer time constraints, we would have liked to observe its behavior after another hour. And most interestingly, we are perplexed by the behavior of our “reverse” solar cell, sample QDSC 6. If its voltage was caused by an electrochemical reaction, it does not explain why it is light-sensitive and its voltage drops to 0 under light.

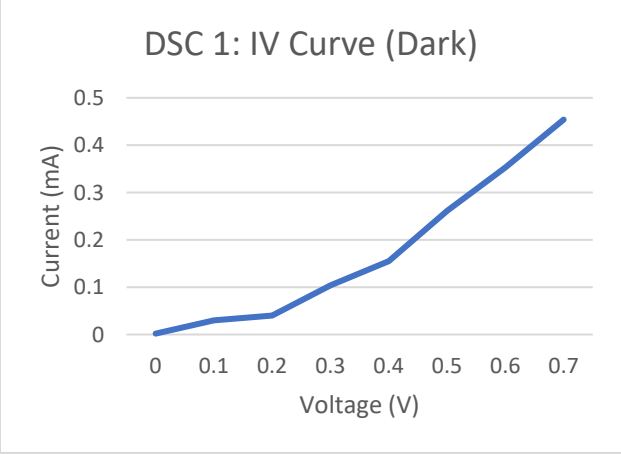

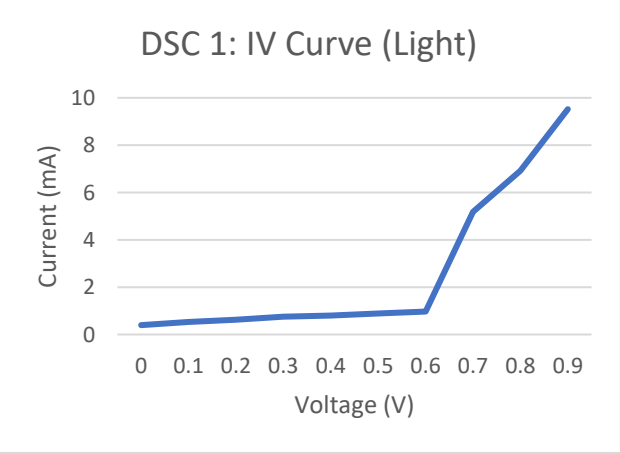

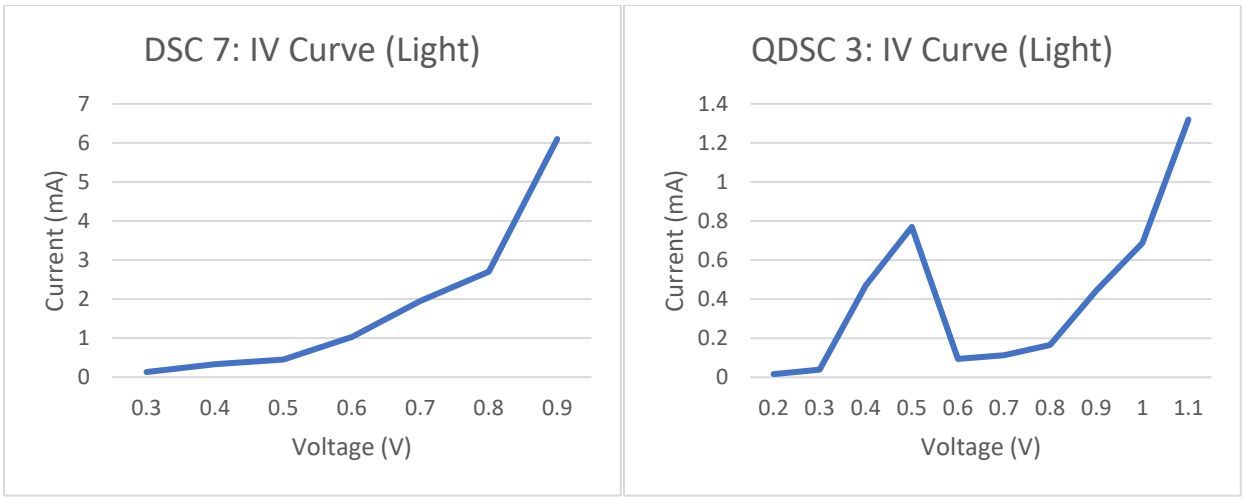

Figure 2.8: IV curves for samples DSC 1, DSC 7, and QDSC 3

Figure 2.8 shows the IV curves for 3 of the samples listed above. We collected these curves because they provide a lot of information about the solar cell, including maximum power, fill factor, and efficiency. However, we were not able to extract this information form the IV curves shown in Figure 2.8 because they do not follow the ordinary behavior of solar cells. Figure 2.9 below shows what a typical IV curve would look like for a solar cell.

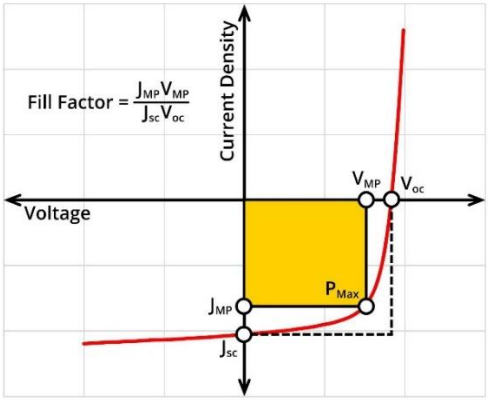

Figure 2.9: Typical IV curve behavior of a solar cell

Ordinarily from the IV curve, voltage at max power (V_{MP}) and current at max power (I_{MP}) can be used with the P_{IN} calculated earlier to find efficiency. We would use;

$$FF = \frac{V_{MP} * I_{MP}}{V_{OC} * I_{SC}}$$

And,

$$Efficiency = \frac{FF * V_{OC} * I_{SC}}{P_{IN}} = \frac{V_{MP} * I_{MP}}{P_{IN}}$$

Since our data does not allow for these calculations, we instead rely on our findings from Table 1.

3 CONCLUSION

Ultimately, we've found that there are a number of combinations and variations employable in quantum dot solar cells to attempt to increase efficiency. While certain features (such as a certain electrolyte) may seem like it does not work in QDSCs, we've found that pairing it with different blocking layers, counter electrodes, or various other layers may actually restore its functionality. Additionally, our results showed very interesting behavior when the solar cells were paired with the polysulfide electrolyte. In the future, we would like to further explore this experiment with at least 5 samples of each structure we created to see which data is consistent and which is based on error. Furthermore, we would like to further test our samples with other methods to determine whether the voltage difference was due to an electrochemical reaction. Ideally, we would also have more time to obtain a proper IV curve to be able to calculate PCE and FF.

Looking forward, we've found that quantum dots have extreme use for solar cells. Most impressively, colloidal QDs have demonstrated multiple exciton generation (MEG), meaning each incoming high energy photon can result in multiple excitons (electron-hole pairs) rather than just one. Previously, the maximum efficiency of a single-layer photovoltaic cell was predicted to be 33.7% by the Shockley-Queisser limit under the assumption that only one exciton can be generated per photon, and remaining energy is lost as electron-photon coupling (vibrations). However, in 2005, NREL was able to push the maximum theoretical efficiency to 65% by demonstrating that QDs exhibited MEG and could produce three electron excitations per photon. This accomplishment highlights the potential for high power conversation efficiency (PCE) in QDs, which has exceeded 16.5% as of 2019. In future endeavors, we would like to see if it is possible to create a quantum dot solar cell with MEG and to measure its efficiency.

4 ACKNOWLEDGEMENTS

All of this would not have been possible without Lu Wang's tremendous support throughout the project. Without her, we would not have been able to coordinate the staff, materials, and procedures we needed for the project. Many thanks for her tireless work.

Special thanks to Adam Cohen for supporting this project and facilitating the experimental portion.

Thank you to David Rose, Thomas Avila, Martin Reiterer, and William Carroll for supporting me through every experimental portion.

5 REFERENCES

[1] P. V. Kamat, "Quantum dot solar cells. The next big thing in photovoltaics.," *The Journal of Physical Chemistry Letters,* vol. 4, no. 6, pp. 908-918, 2013.

[2] V. e. a. González-Pedro, "Modeling high-efficiency quantum dot sensitized solar cells.," *ACS nano,* vol. 4, no. 10, pp. 5783-5790, 2010.

[3] W. W. e. a. Yu, "Experimental determination of the extinction coefficient of CdTe, CdSe, and CdS nanocrystals.," *Chemistry of Materials,* vol. 15, no. 14, pp. 2854-2860, 2003.

[4] E. M. Boatman, G. C. Lisensky and K. J. Nordell, "A Safer, Easier, Faster Synthesis for CdSe Quantum Dot Nanocrystals," *J. Chem. Educ.,* vol. 82, pp. 1697-1699, 2005.

[5] J. e. a. Du, "Zn–Cu–In–Se quantum dot solar cells with a certified power conversion efficiency of 11.6%.," *Journal of the American Chemical Society,* vol. 138, no. 12, pp. 4201-4209, 2016.

[6] Z. e. a. Du, "Optimization of TiO 2 photoanode films for highly efficient quantum dot-sensitized solar cells.," *Journal of Materials Chemistry A,* vol. 2, no. 32, pp. 13033-13040, 2014.

[7] J. G. Radich, R. Dwyer and P. V. Kamat., "Cu2S reduced graphene oxide composite for high-efficiency quantum dot solar cells. Overcoming the redox limitations of S2–/S n 2–at the counter electrode.," *The Journal of Physical Chemistry Letters,* vol. 2, no. 19, pp. 2453-2460, 2011.

[8] H. e. a. Choi, "Highly efficient and thermally stable organic sensitizers for solvent-free dye-sensitized solar cells.," *Angewandte Chemie International Edition,* vol. 47, no. 2, pp. 327-330, 2008.

[9] S. e. a. Giménez, "Improving the performance of colloidal quantum-dot-sensitized solar cells.," *Nanotechnology,* vol. 20, no. 29, pp. 295204-295209, 2009.

[10] Y.-L. a. C.-H. C. Lee, "Efficient polysulfide electrolyte for CdS quantum dot-sensitized solar cells.," *Journal of Power Sources,* vol. 185, no. 1, pp. 584-588, 2008.

[11] N. J. e. a. Cherepy, "Ultrafast electron injection: implications for a photoelectrochemical cell utilizing an anthocyanin dye-sensitized TiO2 nanocrystalline electrode.," *The Journal of Physical Chemistry,* vol. 101, no. 45, pp. 9342-9351, 1997.

[12] A. J. Nozik and R. Memming., "Physical chemistry of semiconductor− liquid interfaces.," *The Journal of Physical Chemistry,* vol. 100, no. 31, pp. 13061-13078, 1996.

[13] K. e. a. Zhao, "Boosting power conversion efficiencies of quantum-dot-sensitized solar cells beyond 8% by recombination control.," *Journal of the American Chemical Society,* vol. 137, no. 16, pp. 5602-5609, 2015.

[14] N. e. a. Guijarro, "CdSe quantum dot-sensitized TiO2 electrodes: effect of quantum dot coverage and mode of attachment.," *The Journal of Physical Chemistry C,* vol. 113, no. 10, pp. 4208-4214, 2009.

[15] G. Halder and S. Bhattacharyya, "Zinc-diffused silver indium selenide quantum dot sensitized solar cells with enhanced photoconversion efficiency.," *Journal of Materials Chemistry A,* vol. 5, no. 23, pp. 11746-11755, 2017.

6 Detailed Experimental Section

6.1 Quantum Dot Synthesis

Colloidal CdSe quantum dots were synthesized using Harvard PS10's Lab 4 procedure which was adapted from [4]. We created the following set-up 4 times to increase the yield of quantum dots.

13mg of CdO and 0.6mL of oleic acid were added to a 25ml flask with a magnetic stir bar and placed over a heating mantle. 10mL of 1-octadecene was added to the flask and sand was poured into the space between the flask and heating mantle to improve heating efficiency. The stir plate was turned on and heating mantle temperature was gradually adjusted as the flask heated. When the reaction was under 110C the variac was set to 85C, when it reached 110C it was reduced to 70C, at 210C it was reduced to 65C, and at 220C it was reduced to 30C. Once the reaction reached 225C, a 1ml sample was taken as a blank for the spectrometer. 1ml of 0.038M selenium solution was added to the flask and a timer was set. After 20 seconds, the reaction was quenched by removing 1ml samples as rapidly as possible into a set of small tubes. This is done to achieve as narrow of a wavelength distribution as possible.

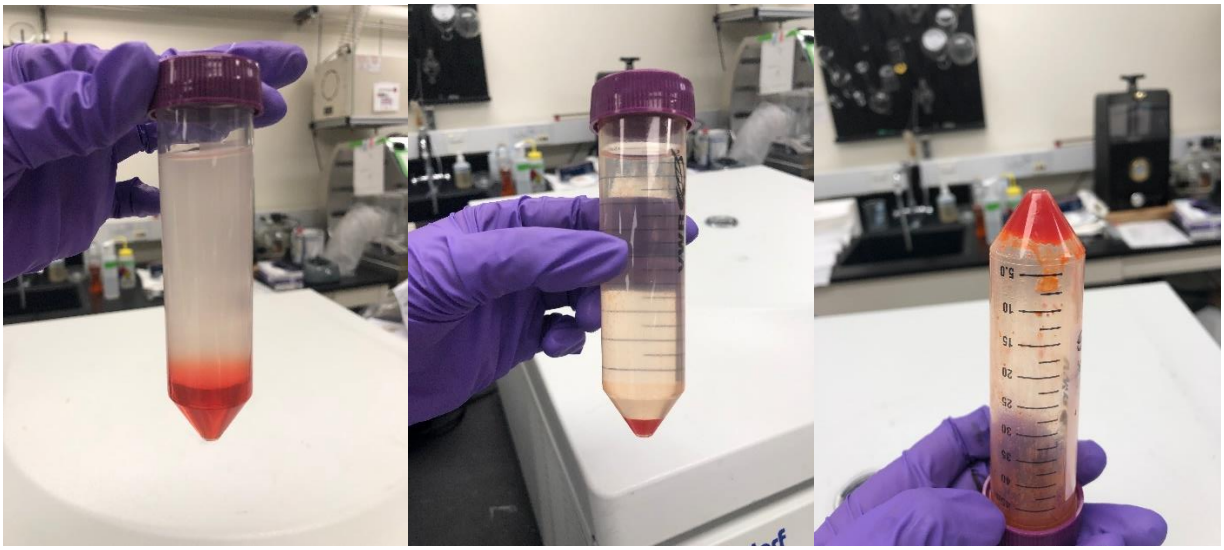

Figure 6.1: The progression of the QD solution as it goes through cycles of ethanol wash to reach isolation

Assuming a 100% reaction conversion efficiency rate, we can estimate the total number of CdSe moles our 4 quantum dot synthesis set ups will produce. In total our reaction consumes 52 mg of CdO (0.4 mmol of Cd) and 4mL of 0.038 M selenium (0.152 mmol of Se) resulting in a maximum of 0.152mmol of CdSe quantum dots.

The first aliquot from each of the four set-ups were first combined to record the absorption spectra. Similarly, this was done with the middle aliquot and the final aliquot to gain a quantitative understanding of the quantum dot wavelength distribution. The variance in peak wavelength for the first aliquot compared to the final one can be explained by the short time difference between quenching the first aliquot versus the last.

All the aliquots were then recombined evenly into two 50mL tubes. For quantum dot purification, a 2:1 ratio of 200 proof ethanal to QD solution was created and centrifuged at 3000rpm for 5 minutes. The top clear layer of the resulting solution was removed and ethanol wash was added to the brim of the tube before centrifuging again. This process was repeated five times before obtaining the purified quantum dots. Approximately 1.126g of (wet) quantum dots were yielded and resuspended in 6ml of dichloromethane.

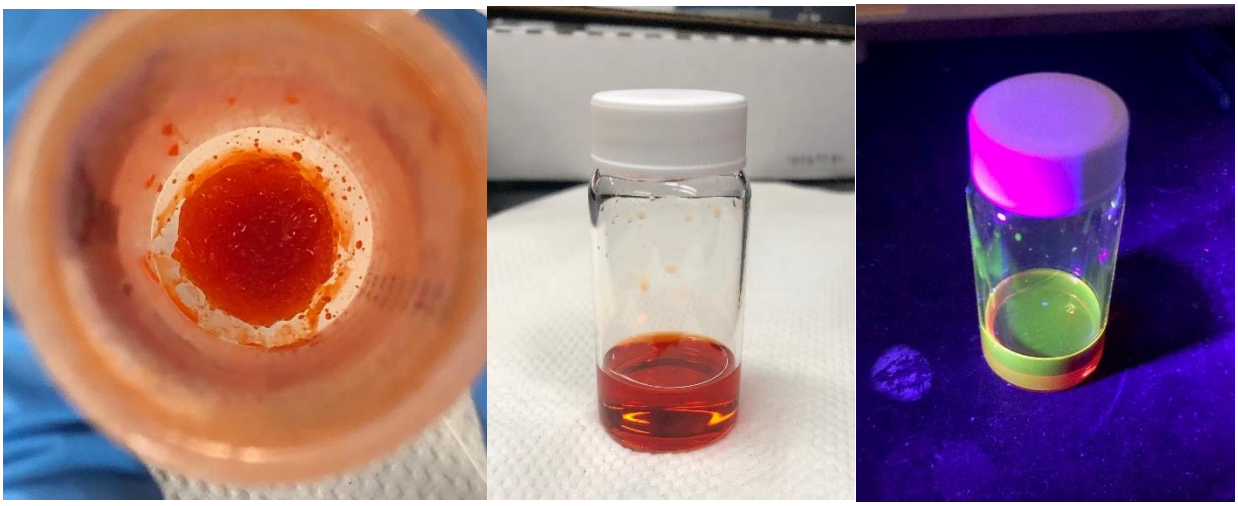

Figure 6.2: From left to right, the purified quantum dots after the final cycle of centrifuging, the QD resuspension in dichloromethane, and the QD-DCM solution under UV light.

Figure 6.2 shows an image of the CdSe quantum dots after the final stage of wash and centrifuging where they appear mostly solid. Under UV light, the final photo in Figure 6.2 shows that the quantum dots solution appears green rather than red. Furthermore, the pH of the final QD-DCM solution was recorded as approximately 4.

6.2 TiO_2 Layers

The procedure used to create the TiO_2 paste was adopted from Harvard's PS1 course, lab 3. In a small vial, mix 1 mL of distilled water and 1 drop of dishwashing soap. In a mortar, mix 6g of commercial Degussa P25 21nm with 9 mL of vinegar and the vial mixture. Let the suspension sit for 15 minutes.

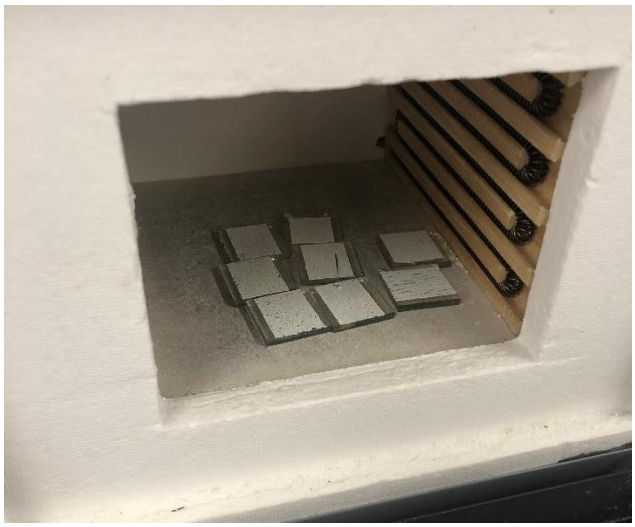

Figure 6.3: OTE slides cast with TiO_2 in a furnace

To cast onto the optically transparent electrode (OTE), tape was applied along the borders of the conductive glass and a doctor blade technique was used to create a thin even layer. Samples were left to bake at 400C for 48 hours. Figure 6.3 shows some of the TiO_2-cast slides prepared. The active area for each slide is approximately 1.5cm by 2.5cm.

To create a scattering layer, an already prepared TiO_2-cast slide was coated with a secondary layer of TiO_2 paste and placed in the oven again for 1 hour.

6.3 Sensitizing TiO_2

To create the dye-sensitized solar cells, a TiO_2-cast slide was immersed in freshly blended blueberry juice for at least 5 minutes, rinsed with water then ethanol, and dried. The slide was then sandwiched with a counter electrode as quickly as possible to prevent oxidization of the dye.

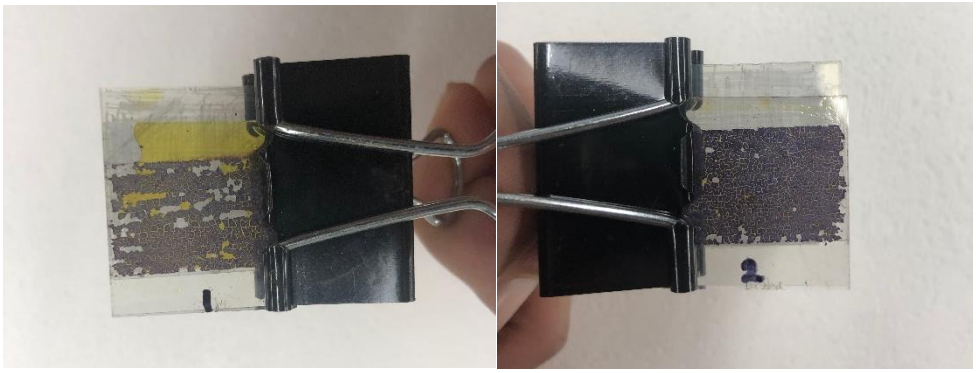

Figure 6.4: Assembled dye-sensitized solar cells

To sensitize the TiO_2 with the CdSe quantum dots, the slides were directly immersed in the DCM-QD solution for 48 hours as shown in Figure 6.5. They were then allowed to dry in air for a few minutes and gently dabbed with Kim Wipes.

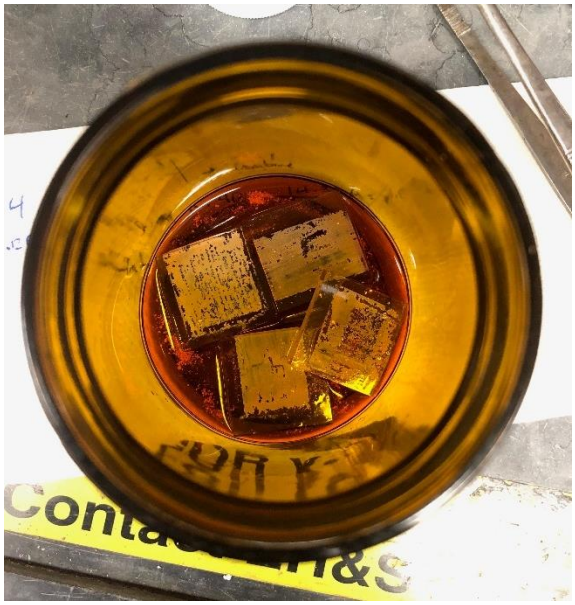

Figure 6.5: TiO2-cast slides immersed in a quantum dot-dichloromethane solution.

6.4 Blocking Layer

To create a ZnS blocking layer, a similar procedure was adapted from [5]. A sensitized TiO_2 conductive slide was immersed in 0.1 M zinc acetate methanol solution for 1 minute, then rinsed with distilled water, immersed in 0.1 Na_2S aqueous solution for 1 minute, and rinsed with distilled water. This process was repeated 5 more times to successfully a deposit a ZnS blocking layer.

6.5 Electrolyte Redox Couple

The iodide electrolyte solution used in this procedure was a pre-prepared stock from Harvard's PS1 chemistry class. To create the polysulfide redox couple electrolyte, a 7:3 methanol to water ratio was used as the solvent for 0.5M Na2S, 2M S, and 0.2M KCl. A magnetic stir bar was placed in the solution and left to mix for at least 10 minutes.

6.6 Counter Electrodes

To create the graphite counter electrode, an even layer of graphite was applied by drawing on the conductive side of an OTE with a number 2 pencil.

To create the copper sulfide counter electrode, a thin 2cm by 2cm sheet of brass was immersed in 3 M hydrochloric acid at 70C for 5 minutes and subsequently immersed in a polysulfide solution (as prepared above) for 10 minutes.

To create the silver counter electrode, a few drops of 3 M silver nitrate were evenly dispersed on the conductive side of an OTE and baked at 375C for 50 minutes.

6.7 Assembly

For assembly, the finalized photoanode and the counter electrode were sandwiched together with a 2mm offset and clamped together with a small binder clip. A few drops of a redox couple electrolyte was applied at the meeting edge of the two electrodes. The electrolyte saturated the TiO_2 layer through capillary action.

6.8 Characterization

To characterize the solar cells, the voltage produced by the cell was measured in the dark, under ambient light (room lighting), and under a 250V 660W incandescent light bulb. The illuminance of the light bulb exposed to the samples was measured with a light meter to be 765 lux or 0.00011169 watts/cm^2. The device output voltage was measured by attaching either edge of the multimeter leads to the photoanode and the counter electrode of the solar cell.

To record a current-voltage (IV) curve of the solar cell, the following set up shown in Figure 6.6 was used to sweep through a series of voltages while recording the current of the cell.

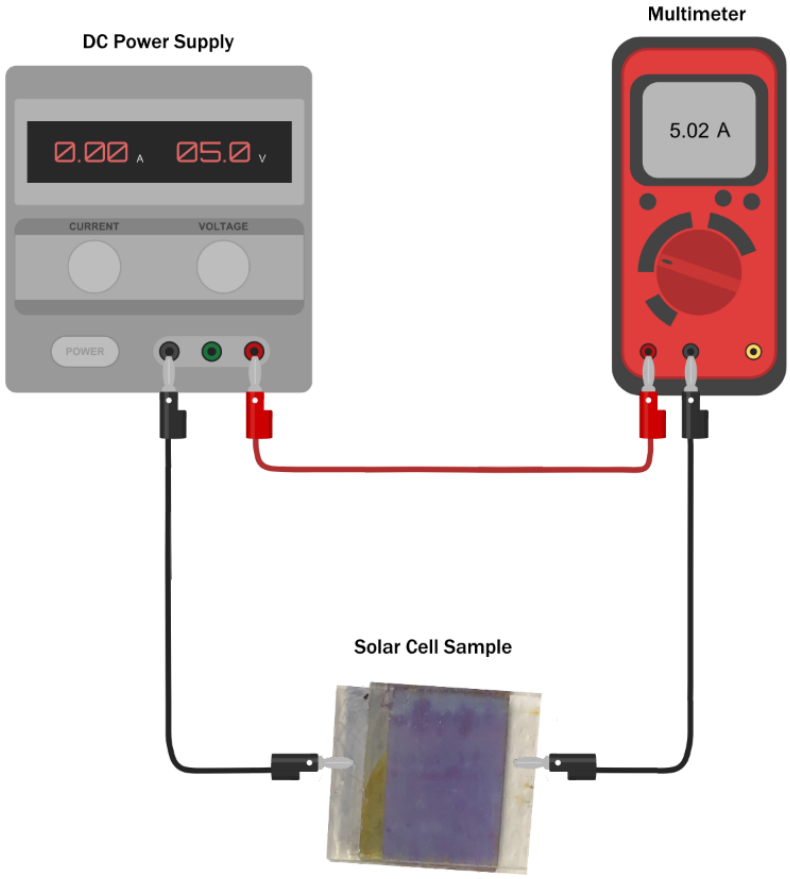

Figure 6.6: Diagram of the set-up used to sweep through voltages to obtain the solar cell IV curve

6.9 Other Recommendations

The experimental procedure we followed was based on the time and resource limitations of the project. There is an abundance of literature which details alternative methods for constructing each layer of the quantum dot solar cell, as summarized below.

TiO_2. To prepare both of the TiO_2 pastes used for the active layer and the scattering layer, [6] details a highly efficient and thorough preparation process. The active layer is created by casting a 5-10um thick mesoscopic oxide film using 15-20nm particles of either TiO_2, ZnO, or SnO_2. Nearly all recent literature on QDSCs use TiO_2 for its higher efficiency.

Creating the compact TiO_2 layer is customarily done by pouring an aqueous solution of 40mM $TiCl_4$ over the surface of the photoanode and treating at 70C for 30 minutes [7] [8].

QD Deposition. There are a number of ways to deposit QDs onto the active TiO_2 layer. This step is done after casting the aforementioned TiO_2 layers.

(1) Drop Cast/Spin Coat – pour colloidal QD suspension on the photoanode surface and dry the film.
(2) Chemical Bath Deposition – this process grows QD sensitizers directly on the TiO_2 film. Typically, an annealing step is added to introduce crystallinity.
(3) Surface Ionic Layer Adsorption and Reaction (SILAR) – successively dip the photoanode through a cycle of chemicals that foster the growth of crystallites directly onto the electrode. The growth is controlled by the number of cycles and the time of each step. Typically, an annealing step is added to introduce crystallinity in this process as well. Gonzalez describes a particular procedure in [2].
(4) Electrophoretic Deposition – immerse two electrodes in a mixed polar/nonpolar solvent and apply an electric field to negatively charge the QDs and drive them into the photoanode. A voltage of 60V is appropriate and the reaction can run for over 30 minutes.
(5) Molecular Linker – deposit QDs to the TiO_2 layer using a bifunctional linker molecule to create sub-monolayer coverage while minimizing particle aggregation. The linker functions through its carboxylic acid group which complexes with the TiO2 and its thiol group which interacts with the QDs [1]. For this process, immerse the photoanode in a molecular linker (such as 3-mercaptopropanoic acid) for 24 hours and then transfer to a toluene-QD solution for a number of hours.
(6) Direct QD adsorption – the photoanode is immersed directly into a colloidal QD dispersion (usually either toluene or CH_2Cl_2) for at least 24 hours (usually 48 hours or more).

The chemical bath and SILAR processes provide very close contact between QDs and the TiO_2 surface, but the QDs tend to be lower quality and higher defects [1]. Electrophoretic deposition allows for more precise size selectivity. The molecular linker and direct QD adsorption processes require less equipment because they employ direct immersion into a prepared colloidal QD solution, but the deposition density is lower. For a molecular linker, the distance of the interaction between the TiO_2 and the QD surface is determined by the linker length. There is less literature employing the drop cast/spin coat process.

Blocking Layer. For the blocking layer, the literature often uses ZnS. Most commonly, the photoanode is coated in multiple ZnS passivation layers by alternately dipping the electrode into zinc acetate and sodium sulfide. Furthermore, an additional blocking layer of SiO_2 may be coated using a similar process.

Combining a ZnS and SiO_2 blocking layer exhibits higher charge collection efficiency compared to ZnS alone [5].

Counter Electrode. There are many options for the counter electrode, some of which pair better with particular electrolyte redox couples. A Cu_2S counter electrode demonstrated 4% PCE in [2] and can be fabricated by immersing brass in HCl and subsequently polysulfide solution. The Cu_2S electrode is particularly important when using the polysulfide electrolyte because it has been shown to exhibit high electrocatalytic activity for polysulfide reduction which increases device performance. Beyond that, the counter electrode material mainly dictates the device's fill factor. A Cu_2S counter electrode experiences a much lower charge transfer resistance between it and the redox couple, so it performs much better than an Au or Pt counter electrode (by a factor of 3 when comparing to Pt) [9].

Alternatively, a Cu-RGO material is cast onto a fluorine doped tin oxide electrode in [7] as the counter electrode. Incorporation of reduced graphene oxide (RGO) in QD films (by casting TiO_2 films that contain RGO) increases efficiency more than 3-fold because the RGO serves as a conduit to transport electrons and improves charge separation in the semiconductor films. Polysulfide electrolyte is necessary to provide stability to the cadmium chalcogenide photoanode, but it introduces undesirable reactions at the counter electrode. The RGO-Cu_2S composite is necessary to transport electrons more effectively, improving the fill factor by about 75%.

Alternatively, a silver nitrate coated counter electrode (mainly FTO) employs a simple fabrication process, evenly placing a few drops of silver nitrate and treating at 375C for 1 hour, and catalyzes the recombination of electrons into the electrolyte, increasing cell PCE.

Electrolyte. Nearly all recent literature on QDSCs employ a polysulfide electrolyte, however a few choose an iodide electrolyte instead. The biggest disadvantage of the I^-/I_3^- redox couple is its corrosive reaction to most metals and semiconductors, causing decay in QDs and a rapid linear decrease of photocurrent.

The performance of a QDSC using only Na_2S as an electrolyte is less than that of an iodide-couple electrolyte. However, the dissolution of Na_2S with sulfur salt S leads to the formation of polysulfide as well as supersulfide ($S_2^{\cdot-}$) which acts as a far superior redox couple for QDSC performance. The polysulfide acts as an electron acceptor from the counter electrode through this reaction:

$$S_x^{2-} + 2e \rightarrow S_{x-1}^{2-} + S^{2-}$$

Based on the results from [10], compared to the I-/I3- iodide electrolyte, the polysulfide had a much higher short-circuit current (ISC) and IPCE values but lower values of FF and open-circuit voltage (VOC). Thus, the efficiency for the polysulfide device was 1.15% compared to 1.84% for the iodide device. A low FF and VOC are indicative of a low hole-recovery rate which increases charge recombination; however, these devices did not have the added ZnS blocking layer designed to mitigate recombination, nor did they have a metal-chalcogenide (such as Cu2S) counter electrode which has been shown to have high electrocatalytic activity for polysulfide reduction resulting in higher stability and performance [7]. These measures limit the back-electron transfer caused by polysulfide's poor charge transfer rate. The lower ISC in the iodide devices indicate that the quantum dots are being degraded by the electrolyte which is also reflected in the device's steady decrease in performance after each measurement.

7 MATLAB THEORETICAL MODELS

7.1 OPTIMIZING ACTIVE TIO2 LAYER THICKNESS: RANDOM WALK

Recent QD literature has shown that an active TiO_2 layer is most effective at a thickness of about 2-10um. A thicker layer allows for the absorption of more light, but it comes at the cost of increasing the length of the pathway for electrons traveling from QDs to the photoanode. Using a Boltzmann distribution, we are able to model the flow of electrons through the active TiO_2 layer as a random walk.

To model the flow of electrons through the TiO2 active layer, we simulate the Brownian forces on an electron by random numbers. To do this, we generate a vector containing 100 random numbers drawn from a Gaussian distribution with mean zero and variance 1. These numbers will constitute a series of random Brownian forces on an electron in the TiO2 layer. Thus, f(j) is the force on the particle at time step j and each force displaces the particle by an amount proportional to said force. The scale of this time step remains undefined because it is difficult to quantify the charge-transfer kinetics of any given TiO2 layer. A particular scale may be assigned to this time step if the charge-transfer kinetics of the TiO2 layer can be defined.

Furthermore, in this model, we choose a proportionality constant of 1. However, depending on the properties of the TiO2 layer and the respective charge-transfer kinetics, this proportionality constant can be adjusted as well.

The total displacement of the electron is the sum of the displacements due to the force at each time step. This trajectory is called a "random walk". In Figure 7.1 we illustrate what this random trajectory may look like for a single electron.

```
f = randn(100,1);

h  = cumsum(f);
t = linspace(0, 99, 100);
plot(t, h)
title('Total Displacement')
xlabel('Time')
ylabel('Cumulative Displacement')
```

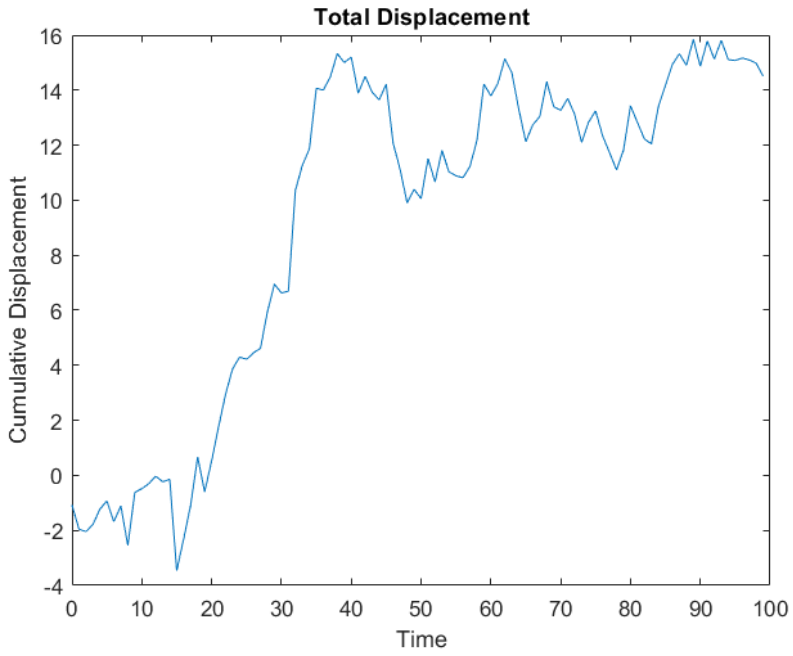

Figure 7.1: Random walk trajectory simulation for a single electron

To gain a more cohesive understanding of the behavior of electrons undergoing this random walk and the effect of the thickness of the TiO2 layer, we model and simulate the trajectories of electrons through varying TiO2 layer thicknesses. There are two critical variables that must be optimized to maximize the number of electrons that move beyond the TiO2 layer in a given time t: the number of photons absorbed by the layer and the travel time of electrons through the layer. Although smaller thicknesses reduce the travel time of electrons, the number of photons absorbed by the TiO2 layer scales up with thickness. However, the factor by which it scales also experiences an exponential decay. Meaning, at very small thicknesses, an additional micron in thickness would increase the number of photons absorbed by a large factor. However, at large thickness, an additional micron would only increase the number of photons absorbed by small amount. For this model, we can approximate the relationship between photons and thickness as linear.

To create this, we assume that for every micron of thickness, the TiO2 is able to absorb 1000 photons. Therefore, a 2um layer would absorb 2000, and a 10um layer would absorb 10000 photons.

To give an image of what this would look like, we first model the electron trajectories of a 1um thick layer which absorbs 1000 photons over the course of 100 time steps. Figure 7.2 below demonstrates the results of the trajectories of 200 of these electrons.

```
h = cumsum(randn(100,1000))/3;
plot(t, h(:, 300:500))
title('Total Displacement')
xlabel('Time')
ylabel('Cumulative Displacement')
```

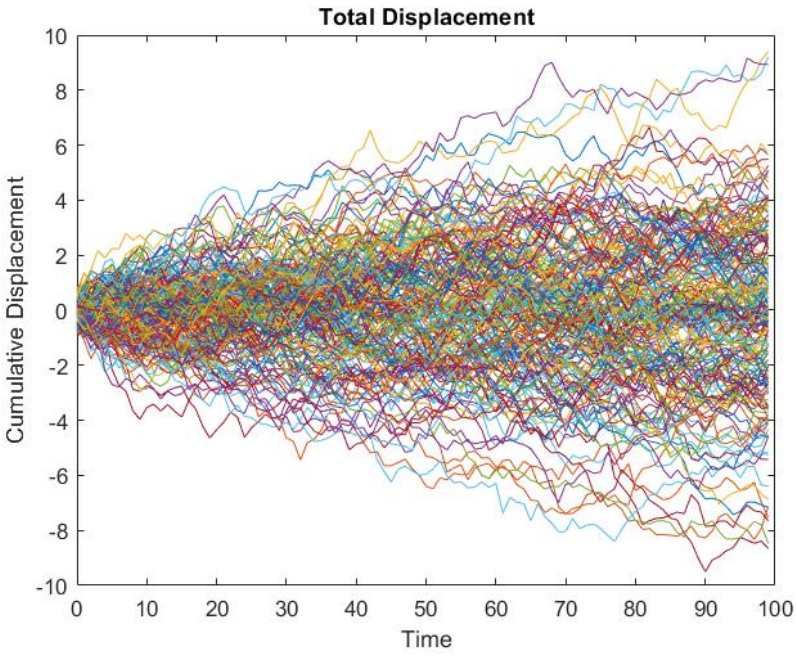

Figure 7.2: Random walk trajectory simulation for 200 electrons

To determine the number of electrons which were able to travel beyond the TiO2 layer, we count all the electrons that have a cumulative displacement greater than 1um.

```
Count = sum(h(100,:)>1)
```

```
Count = 381
```

Now we simulate the distribution of how far the 1,000 electrons have diffused through the TiO2 layer as a function of time. We create a histogram of the distribution of electron positions at times t = 5, 10, 20, 50, 100.

```
xHist = histc(h', -50:50);
plot(-50:50, xHist(:,[5, 10, 20, 50, 100]))
xlabel('Displacement')
ylabel('Number of particles')
```

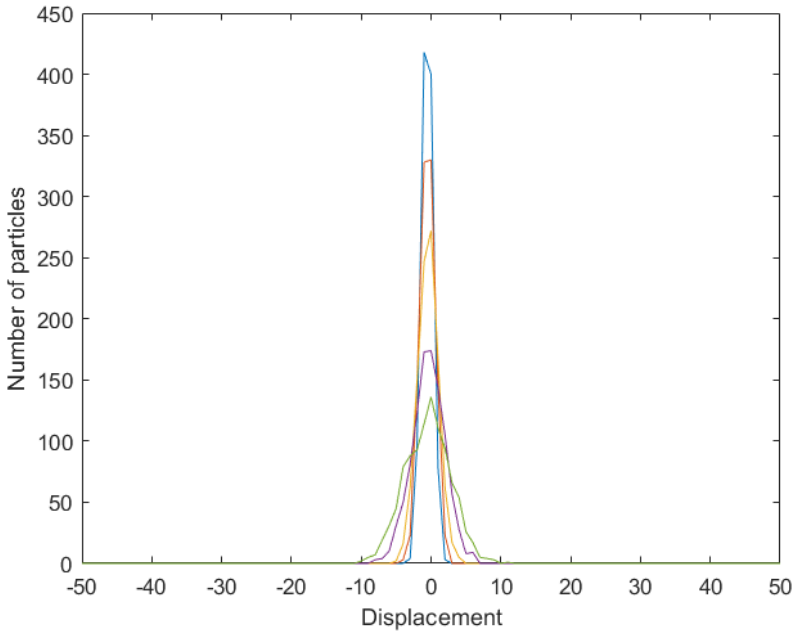

Figure 7.3: Diffusion distribution of 1,000 electrons through a TiO2 layer as a function of time. Blue t=5, orange t=10, yellow t=20, purple t=50, green t=100.

The distribution of electron displacement in Figure 7.3 follows a gaussian distribution. It seems as though as time goes on, half the electrons travel in the right direction to reach the photoanode whereas the other half would experience recombination, one of the biggest limiting factors of QDSC PCE.

To determine how broad this distribution actually is, we calculate the standard deviation of the electron positions at each time step and we plot this as a function of time.

```
stddev = std(h');

plot(t, stddev)
xlabel('Time')
ylabel('Standard Deviation')

plot(t, stddev.^2)
xlabel('Time')
ylabel('Standard Deviation Squared')
```

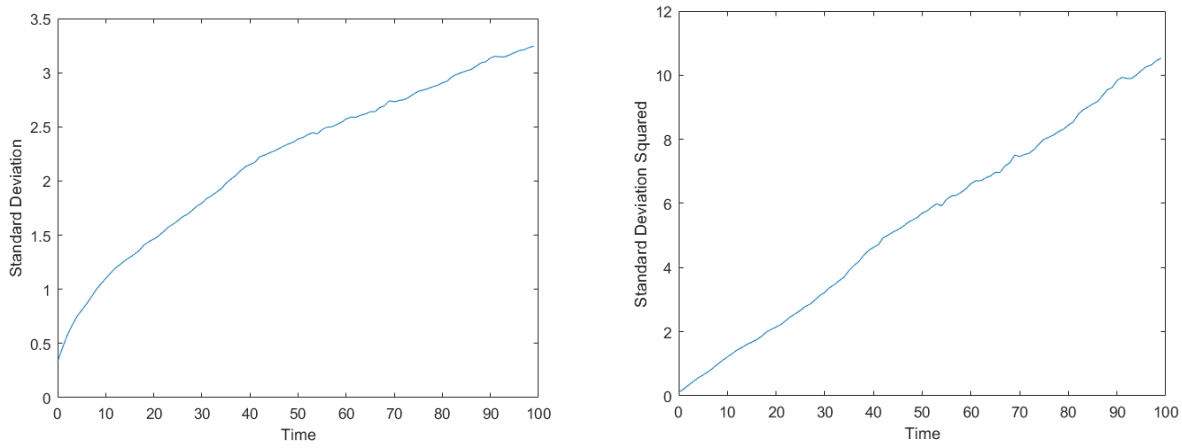

Figure 7.4: Standard deviation of electron displacement as a function of time. On the left, standard deviation vs. time. On the right, standard deviation squared vs. time.

To determine the precise relationship between standard deviation of position and time, we take the square root of standard deviation and plot this against time. This reveals that the distance traveled can be approximated as the square root of time, as shown in Figure 7.4.

Now that we have established a relationship between the thickness of the TiO2 layer with both the time it takes electrons to travel and the number of photons it will absorb, we can finally begin to create a model that optimizes TiO2 thickness. For this, we will compare the number of electrons that surpass the TiO2 layer given thicknesses varying from 1um to 10um.

First, we model the trajectories of all the photons in each TiO2 layer. We account for the fact that the number of photons in each layer must be proportional to the layer's thickness.

```
h1 = cumsum(randn(100,1000))/3;
h2 = cumsum(randn(100,2000))/3;
h3 = cumsum(randn(100,3000))/3;
h4 = cumsum(randn(100,4000))/3;
h5 = cumsum(randn(100,5000))/3;
h6 = cumsum(randn(100,6000))/3;
h7 = cumsum(randn(100,7000))/3;
h8 = cumsum(randn(100,8000))/3;
h9 = cumsum(randn(100,9000))/3;
h10 = cumsum(randn(100,10000))/3;
```

In order to determine whether an electron has traveled beyond the TiO2, its cumulative distance at time t=100 must be equal to or greater than the layer thickness.

```
Count1 = sum(h1(100,:)>1)
```

Count1 = 382

```
Count2 = sum(h2(100,:)>2)
```

Count2 = 559

```
Count3 = sum(h3(100,:)>3)
```

Count3 = 581

```
Count4 = sum(h4(100,:)>4)
```

Count4 = 499

```
Count5 = sum(h5(100,:)>5)
```

Count5 = 307

```
Count6 = sum(h6(100,:)>6)
```

Count6 = 215

```
Count7 = sum(h7(100,:)>7)
```

Count7 = 109

```
Count8 = sum(h8(100,:)>8)
```

Count8 = 68

```
Count9 = sum(h9(100,:)>9)
```

Count9 = 34

```
Count10 = sum(h10(100,:)>10)
```

Count10 = 17

From this model, we find that the optimal TiO2 thickness would be 3um, which allows approximately 581 electrons to travel past the TiO2 layer and reach the photoanode. However, it is important to note some of the limitations of this model. Most importantly, our data does not model realistic or accurate proportionality constants. The proportionality constant chosen for the Brownian forces, as mentioned before, was chosen arbitrarily. Similarly, the assumption that 1um of thickness allows for absorbance of 1000 photons was also chosen arbitrarily and instead models the relative relationship between different TiO2 layer thicknesses and absorbance. Finally, the time step that we have chosen to be t=100 is another arbitrary choice that would have to be scaled appropriately to the accurate charge-transfer kinetics of the TiO2 layer. Furthermore, our simulation does not account for electron accumulation within the semiconductor which ordinarily would create a potential gradient within the TiO2 and would affect the quasi-Fermi level.

7.2 Blocking Layer: Random Walk with Reflecting Barrier

As mentioned in the Active TiO2 Layer model, the distribution of electron displacement reveals that electrons have equal probability of traveling in the correct direction to reach the photoanode or the opposite direction to experience recombination, one of the biggest limiting factors of QDSC PCE. The charge-transfer kinetics of the hole transfer are 2-3 orders of magnitude slower than the QD to TiO2 electron transfer, so employing an effective antidote for recombination could increase QDSC PCE most drastically. Fortunately, the blocking layer in QDSCs was introduced to address this issue. The blocking layer prevents back electron transfer from the QDs and TiO2 particles into the redox couple, thereby minimizing recombination losses at grain boundaries. The effect of the blocking layer can be modeled as adding a reflecting barrier to the "random walk" simulation demonstrated above (in the Active TiO2 layer thickness model). Of course, this is an idealized model which does not account for the efficiency of the blocking layer and the electrons that may still experience recombination. However, with a “perfect” blocking layer, we would expect electrons to behave as described in this model.

To model the effect of the blocking layer, we suppose that electrons in the TiO2 layer begin at position 0 and the impenetrable reflective barrier is placed at a position of -5. We assume that the photoanode is at a positive position greater than 0. The absolute values of these parameters are arbitrary and can be adjusted to more accurately model a QDSC based on the thicknesses, properties, and types of blocking layers it uses.

If an electron hits the impenetrable blocking layer, it will be bounced in the opposite direction where Brownian forces will continue affecting its trajectory. We model the trajectories for 1,000 electrons starting at position 0 for 2,000 time steps, and we plot the trajectories of 50 random electrons in Figure 7.5.

```
tMax = 2000;
t;
N = 1000;
h = cumsum(randn(tMax,N));

for i = 1:tMax
   for j = 1:N
      h(i,j) = abs(0 - h(i, j));
   end
end

t = linspace(0, tMax, tMax);
plot(t, h(:, 300:350))
title('Total Displacement')
xlabel('Time')
ylabel('Cumulative Displacement')
```

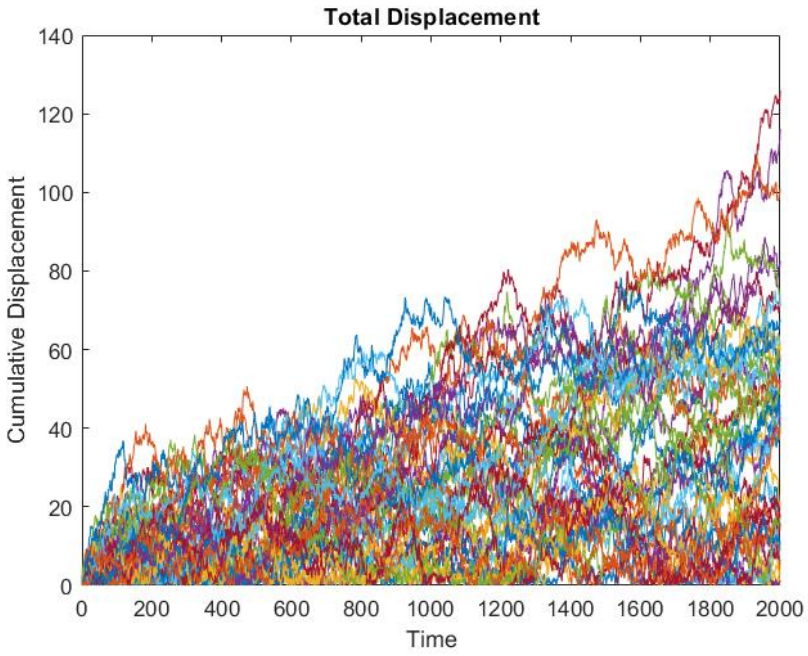

Figure 7.5: Random walk trajectories of 50 random electrons in the presence of a reflective barrier (blocking layer)

We also plot histograms of the distribution of positions at t = 5, 30, 100, 300, and 100 in Figure 7.6.

```
xHist = histc(h', -5:100);

plot(-5:100, xHist(:,[5, 30, 100, 300, 1000]))
xlabel('Displacement')
ylabel('Number of particles')
```

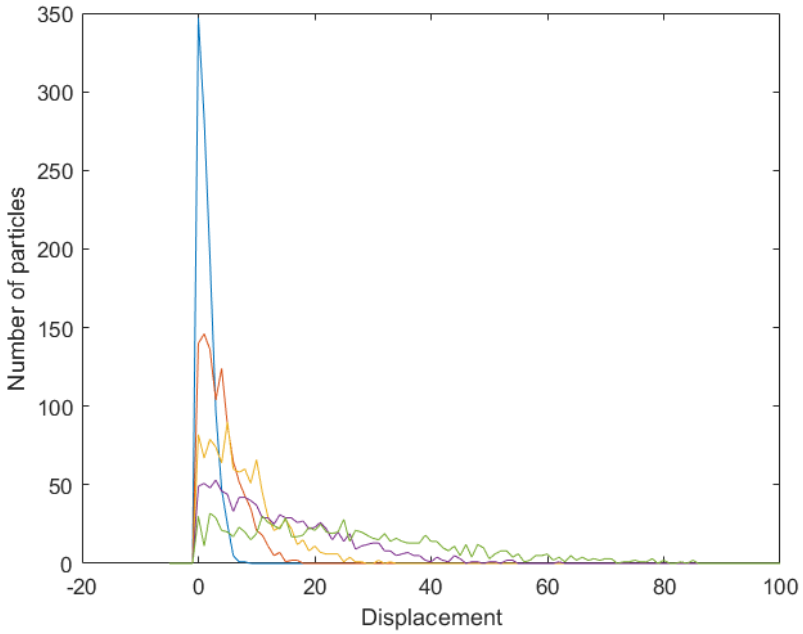

Figure 7.6: Distribution of trajectories of 1,000 random electrons in the presence of a reflective barrier (blocking layer)

Unlike the simulations above that exclude a blocking layer, almost all of electrons in this case are in the correct and positive direction toward the photoanode. Very few electrons remain in the area between positions -5 and 0, and the fraction of them which do decreases with time. This demonstrates the critical importance of a blocking layer in minimizing recombination and electron loss for increased cell PCE.

7.3 The Solar Spectrum and the Shockley-Queisser Limit

To better understand the solar spectrum that all solar cells, including QDSCs, are designed to accommodate, we model the "standard solar spectrum" to determine estimates of photon flux at different wavelengths and the ideal semiconductor bandgap.

To model quantum dot response to the solar spectrum, we will use data from a group which has defined a standard solar spectrum. This spectrum is plotted below in Figure 7.7.

```
data = readtable('ASTMG173.csv');

lambda = data.Wavelength_nm;
ETS = data.ETS;
TS = data.Circumsolar;
plot(lambda, ETS, lambda, TS, 'r');
xlabel('Wavelength (nm)');
ylabel('Intensity (W m^{-2} nm^{-1})');
```

```
title('Solar Spectrum');
legend('ETS', 'TS');
```

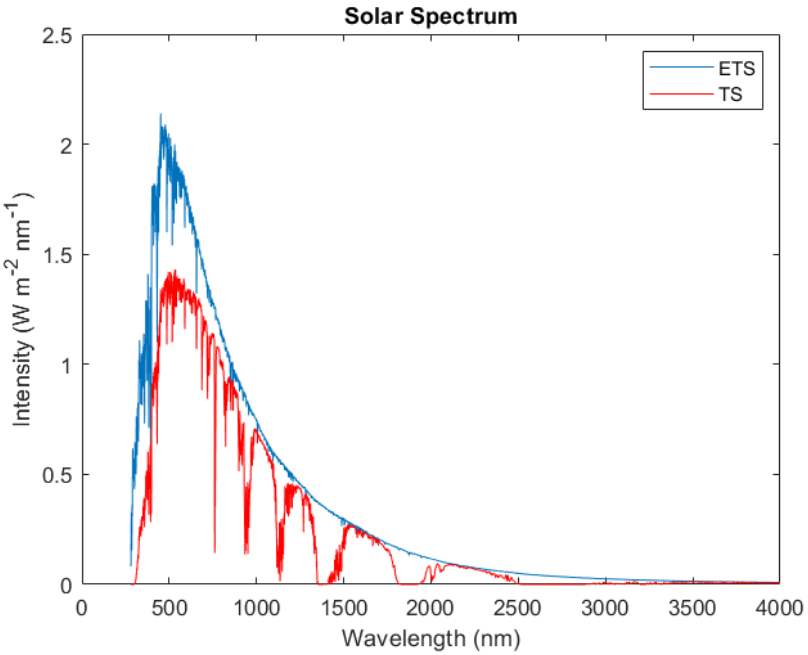

Figure 7.7: Model of the solar spectrum

We also model the total solar intensity arriving at the surface of the earth based on the aforementioned solar spectrum data.

```
dlambda = lambda(2:end) - lambda(1:end-1);
areas = dlambda.*TS(2:end);
```

The total solar radiation intensity we calculate is: 899.6 $\frac{W}{m^2\ nm}$.

```
solar_rad_intensity = sum(areas);
```

To calculate the maximum efficiency of a single-junction solar cell (that does not experience MEG), we first establish that the voltage a solar cell produces is proportional to the bandgap of the sensitizer. In order to excite electrons in the sensitizer, photons must have energy greater than the semiconductor band gap, otherwise the photon is not absorbed, and its energy is lost.

In order to calculate the number of photons hitting the Earth's surface at each wavelength, we relate energy and wavelength with the following equation:

$$E(\lambda) = \frac{hc}{\lambda}$$

From here, we are able to plot photon flux as a function of wavelength as illustrated in Figure 7.8.

```
h = 6.63e-34; %Planck constant in SI
```

```
c = 3e8; %Speed of light in SI
ephot = (h*c*1e9)./(lambda); % vector of the energy at each wavelength

nphot = TS ./ ephot;

plot(lambda, nphot);
xlabel('Wavelength (nm)');
ylabel('Photon Flux (m^{-2} s^{-1} nm^{-1})');
title('Photon Flux with Wavelength');
```

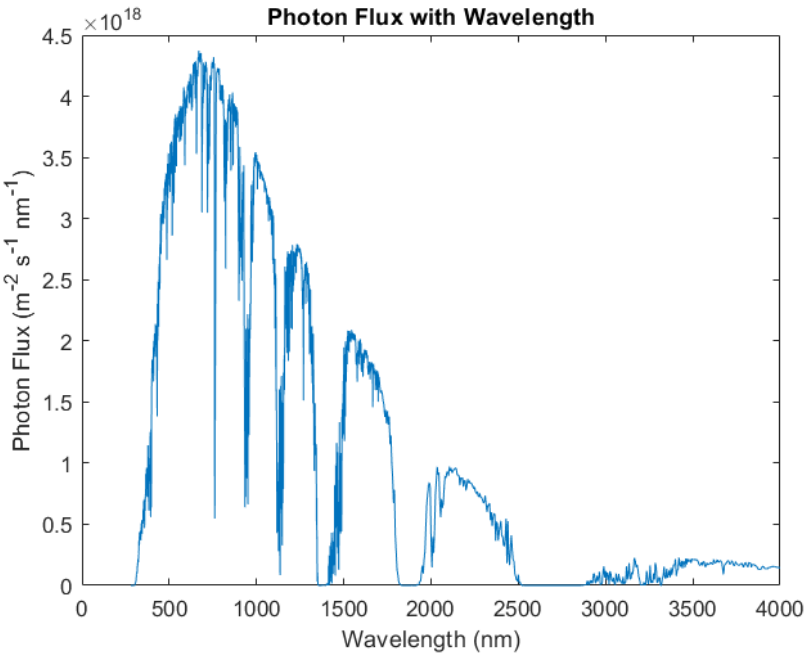

Figure 7.8: Flux of photons onto the Earth's surface based on wavelength

To determine the number of photons that will be absorbed by a sensitizer of any given specific band gap, we calculate for every wavelength the number of photons that have an energy equal to or greater than its corresponding energy. This is illustrated below in Figure 7.9.

```
Nabs = cumsum(nphot(2:end).*dlambda);

plot(ephot(2:end), Nabs);
xlabel('Energy (J)');
ylabel('Photon Absorbed (s^{-1} m^{-2})');
title('Photons Absorbed');
```

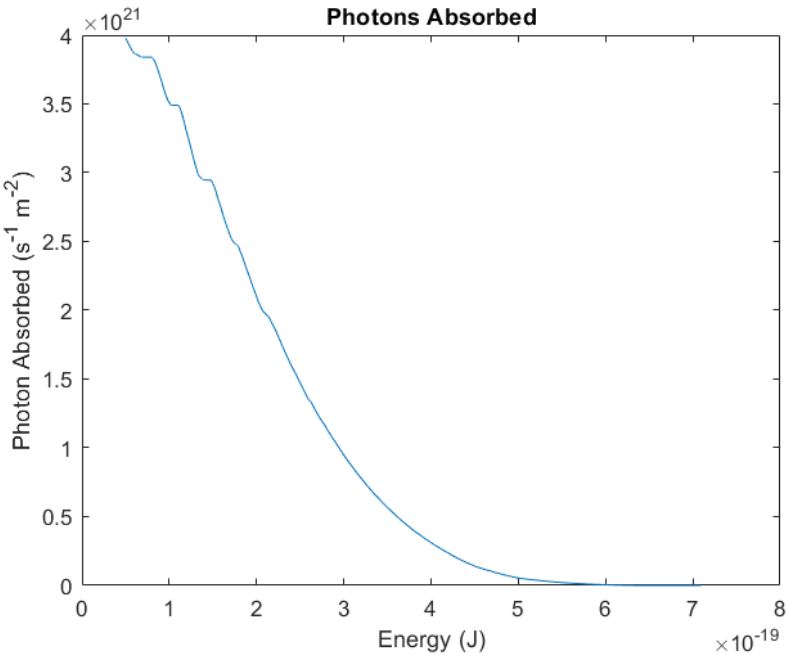

Figure 7.9: Number of photons absorbed by varying energies of bandgaps

As energy increases, the number of photons that have that energy equal to or greater than that decreases. Our QDs have wavelengths ranging 515-535nm which correspond to an energy of approximately 3.7 x 10^-19 J. According to our model, they would absorb a very low fraction of the modeled solar spectrum. However, this comes at the advantage that whichever photons are absorbed will be high energy.

In order to design the optimum bandgap to delivery maximum efficiency, we use the following equation to calculate and plot the most effective bandgap to maximize power out as shown in Figure 7.10.

$$P_{cell} = E \times N_{abs}.$$

```
Pcell = ephot(2:end) .* Nabs;

plot(ephot(2:end), Pcell);
xlabel('Energy (J)');
ylabel('Power (W)');
title('Power of Solar Cell by Bandgap');
```

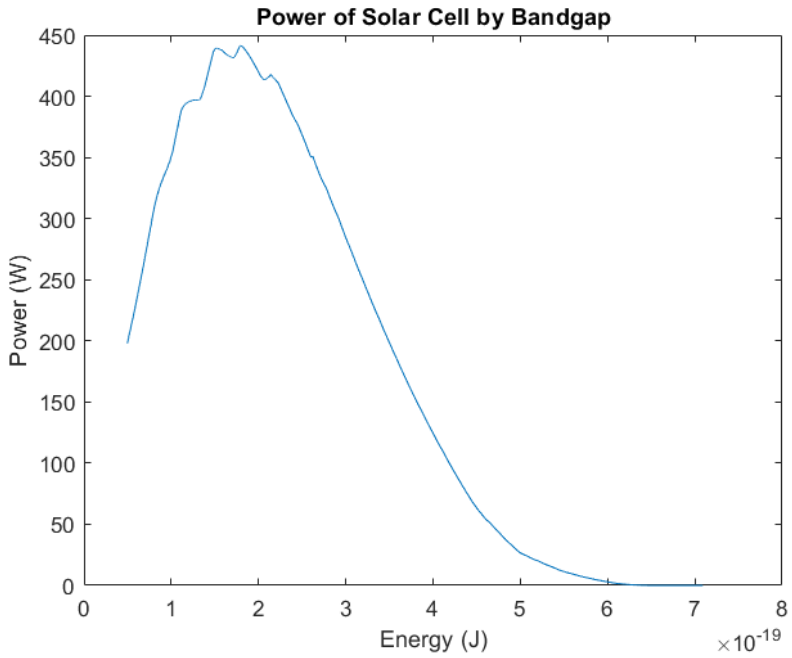

Figure 7.10: Visualization of maximum device power output by varying bandgap energies.

```
[maxPower, index] = max(Pcell);
Bandgap = ephot(index)/1.6e-19; % Band gap in Joules converted to eV
```

The optimum bandgap for maximum power delivery is 1.12 eV with power of 441 $\frac{W}{m^2}$.

```
maxefficiency = maxPower / solar_rad_intensity;
```

Therefore, our model estimates the Shockley-Queisser Limit on maximum efficiency of a single-junction solar cell (defined as the ratio between maximum power and intensity) at 49.06%. The recognized value for this limit in the literature is 33.7%, which accounts for various additional factors which our model simplifies. However, as mentioned before, in addition to fabricating a tandem layer QDSC, it is also possible for quantum dot solar cells to exceed this limit through to their demonstrated ability to undergo MEG.